J. Fluid Mech. (1990), *vol.* 216, *pp.* 505–536
Printed in Great Britain

Wave–current interactions: an experimental and numerical study. Part 2. Nonlinear waves

By G. P. THOMAS
Department of Mathematical Physics, University College, Cork, Ireland

(Received 12 May 1989 and in revised form 14 November 1989)

The interaction between a regular wavetrain and a current possessing an arbitrary distribution of vorticity, in two dimensions, is considered for waves of finite amplitude. A numerical model is constructed, primarily for use in the finite depth regime, extending the work of Dalrymple (1973, 1977) and this is used to predict the wavelength and the particle velocities under the waves. These predictions agree very well with experimentally obtained data and the importance of the vorticity in the wave–current interaction is clarified. Amplitude and wavelength modulations are considered for finite amplitude waves on a slowly varying irrotational current; moderate agreement is found between theory and experiment.

1. Introduction

The interaction between a steady current and a regular progressive wavetrain in two dimensions can only be described via an analytic solution if the waves are irrotational, corresponding to a uniform current or one with a uniform distribution of vorticity. If the current possesses an arbitrary distribution of vorticity then analytical solutions cannot be obtained for either linear or finite-amplitude waves and numerical solutions must be sought. The existing analytical work on wave–current interactions is well documented in the major review by Peregrine (1976) and a briefer more recent review is given by Peregrine & Jonsson (1983). In the later review the authors make a 'state-of-the-art' assessment and conclude that the influence of vertical variation in the current profile, i.e. the vorticity, is as yet poorly understood. This partially represents a lack of existing study for engineering applications, since the model of Thomas (1981) for linear waves on a non-uniform current has been verified experimentally and is simple to implement. Thus for linear waves the method of solution exists; the aim of this paper is to study the case for which the waves are of finite amplitude.

For finite-amplitude waves with an arbitrary distribution of vorticity, the only existing work is due to Dalrymple (1973, 1977), who constructed a numerical model based upon a Dubreil-Jacotin transformation. Examples were given by Dalrymple for a linear shear current and a current similar to a $\frac{1}{7}$-power-law, but one of the drawbacks with the Dalrymple model is that the vorticity distribution is defined in terms of stream-function values and is not a direct function of the vertical coordinate z. More recent numerical work for finite-amplitude waves has been focused on linear current profiles, for which the wave field is irrotational. Simmen & Saffman (1985) considered the case for waves on water of infinite depth with solutions obtained for waves up to and including the limiting waves. An extension to water of finite depth has been made by Teles da Silva & Peregrine (1988). One feature of these numerical models for irrotational waves is that they are computationally very efficient.

There have been two major relevant experimental studies in recent years and both have been primarily concerned with measurement of velocities and wavelengths to demonstrate the practical significance of the interaction between waves and currents. The first study is reported by Brevik & Aas (1980) and by Brevik (1980); measurements were obtained for both rippled and smooth beds but difficulty was experienced in reconciling experimental data with irrotational wave theories. The second set of experiments was conducted by Kemp & Simons (1982, 1983) in a study of the interaction between regular waves and a turbulent current over rough and smooth beds. Particular attention was given to the near-bed region in which exceptionally detailed measurements were obtained. This study is probably the most comprehensive to date and illustrated the interactive mechanism between the waves and current very dramatically. Both of the studies were within the near-linear regime and wave effects higher than second order were not considered. In addition comparison with wave theories was limited to irrotational waves; in most of the current profiles presented the vorticity showed a variation with depth and this would very likely prove important if an accurate comparison of theory and experiment were required.

This paper extends the previous work of Thomas (1981) to finite-amplitude waves interacting with a current which possesses an arbitrary distribution of vorticity. For a given mean water depth, wave frequency, wave amplitude and current profile below the wave trough, the theoretical model aims to provide a complete description of the wave kinematics and these are usually represented by the wavelength and the velocity profiles under the wave crest and trough.

The numerical model is based upon the work of Dalrymple (1973, 1977) and includes the current as a function of the vertical depth coordinate. To implement this depth variation in the current the appropriate relationships between the vorticity distribution and the flow parameters must be determined; these are derived in the earlier part of the paper. The numerical model is then formulated as a constrained minimization problem utilizing the property that the free surface is one of constant pressure. Existing finite-amplitude solutions are used to test the model.

Predictions of the numerical model are compared with experimental data and excellent agreement is found to exist between measured and predicted wavelengths and velocity profiles. From this comparison some important comments can be made upon the influence of the vorticity distribution on the flow kinematics and the applicability of various wave theories, though it should be acknowledged that these restrictions are only deduced for waves in water of finite depth. Finally an attempt is made to place the experimental results in a wider framework by using the Whitham (1974) theory to consider the amplitude and wavelength modulations for a slowly varying flow. Despite the acknowledged presence of vorticity (which has been shown to be relevant to the local kinematics) and laboratory constraints, a surprisingly good degree of agreement was found to exist between the experimental values and predictions using the Whitham theory for irrotational currents.

2. Formulation

A regular wavetrain of plane waves propagates over water of mean constant depth h. The wavetrain is characterized by an amplitude measure a, wavenumber k and frequency ω. Alternatively the wave height H, wavelength $\lambda(=2\pi/k)$ and period $T(=2\pi/\omega)$ could be used.

Cartesian coordinates (x, z) are chosen so that the horizontal x-axis is in the

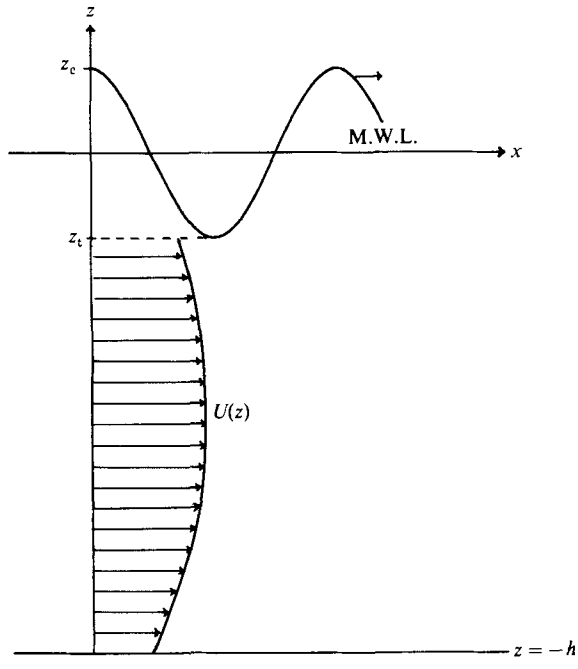

FIGURE 1. Definition of coordinate system.

direction of wave propagation and the z-axis points vertically upwards; the origin lies in the mean water level and the coordinate system is shown in figure 1. The surface elevation of the wavetrain is described by $z = \eta(x,t)$ and the wave troughs and crests correspond to the points at which $z = z_t$ and $z = z_c$ respectively.

For all points below the wave trough the horizontal component of velocity u can be written as a superposition of a time-independent current term and a wave-like term

$$u(x,z,t) = U(z)+u_w(x,z,t), \quad -h \leqslant z \leqslant z_t \tag{2.1}$$

with the average value of u_w over a wave period or a wavelength being zero. This wave-like velocity component can also be written as a harmonic series

$$u_w(x,z,t) = \sum_{n=1}^{\infty} u_n(z)\cos n(kx-\omega t) \tag{2.2}$$

in terms of the phase function $kx-\omega t$, valid for $-h \leqslant z \leqslant z_t$. Between the wave trough and the wave crest, i.e. $z_t < z \leqslant z_c$, the velocity field is well defined but cannot be meaningfully written in a form analogous to (2.1).

The quantities a, ω and h, together with the function $U(z)$, can be regarded as known either from experimental measurements or by specification. Using this information the aim is to predict the wavelength, the surface profile and the velocity field under the waves. The water is assumed to be both incompressible and inviscid but the wavetrain is allowed to be both of finite amplitude and rotational.

2.1. *The stream function* ψ

The formulation can be simplified by changing to a frame of reference in which the origin moves in the direction of propagation of the wave with a speed c equal to the

phase speed of the wave, i.e. $c = \omega/k$. In such a reference frame the wave is stationary and the flow is steady.

For an incompressible fluid in this moving reference frame, the stream function $\psi(x, y)$ is defined by

$$u - c = -\frac{\partial \psi}{\partial z}, \quad w = \frac{\partial \psi}{\partial x}, \tag{2.3}$$

where w is the vertical component of velocity. As the flow is two-dimensional, inviscid and incompressible, an application of Helmholtz's theorem yields

$$\nabla^2 \psi = -\Omega(\psi), \tag{2.4}$$

where Ω is the vorticity distribution in the fluid and is constant along a streamline. This Poisson equation is the governing equation for the flow.

On the bottom boundary $z = -h$, the vertical component of velocity must be zero. Using (2.3) this becomes

$$\frac{\partial \psi}{\partial x} = 0 \quad \text{on} \quad z = -h. \tag{2.5}$$

In the moving reference frame, denote the free surface by $z = \zeta(x)$. The kinematic free-surface condition is readily shown to be equivalent to the statement that the free surface must be a streamline. Hence the kinematic condition becomes

$$\psi(x, \zeta(x)) = \text{constant}. \tag{2.6}$$

The dynamic free-surface condition asserts that the pressure p on the free surface is constant. For an inviscid fluid of constant density ρ in steady motion, Bernoulli's equation states that the quantity $p/\rho + \frac{1}{2}u'^2 + gz$ is constant along a streamline, where $\boldsymbol{u}'$ is the local velocity field. As $\boldsymbol{u}'$ is equal to $(u - c, w)$ and the pressure is constant on the free surface, Bernoulli's equation on the free surface gives

$$\tfrac{1}{2}[\psi_x^2 + \psi_z^2] + g\zeta = \text{constant} \quad \text{on} \quad z = \zeta(x), \tag{2.7}$$

where (2.3) has been used to determine $\boldsymbol{u}'$. The values of the constants in (2.6) and (2.7) are not known or specified at this stage.

The equation (2.4), together with the boundary conditions (2.5)–(2.7), determine the problem for the stream function $\psi(x, z)$ and the surface elevation $\zeta(x)$. Only solutions that are periodic in x with finite period λ are sought; the problem for solitary waves, as $\lambda \to \infty$, has previously been considered by Benjamin (1962). A further condition to be imposed is that the mean value of the surface elevation $\zeta(x)$ over any interval of length λ must be zero; this is a consequence of the origin being chosen to lie at the mean water level.

2.2. *The Dubreil-Jacotin transformation*

There are two main difficulties associated with the formulation outlined above. The first is that the vorticity distribution which appears in the Poisson equation is a function of the unknown dependent variable $\psi(x, z)$. The second is associated with the free surface, which is unknown and not likely to be a shape amenable to general numerical techniques.

To overcome these difficulties the coordinate transformation devised by Dubreil-Jacotin (1934) is introduced. This employs x and ψ as the independent variables and z is regarded as a function of x and ψ. The transformation is shown diagrammatically in figure 2 for a domain of half a wavelength; as the waves are both symmetric and periodic it is not necessary to use a larger domain. The transformed domain is

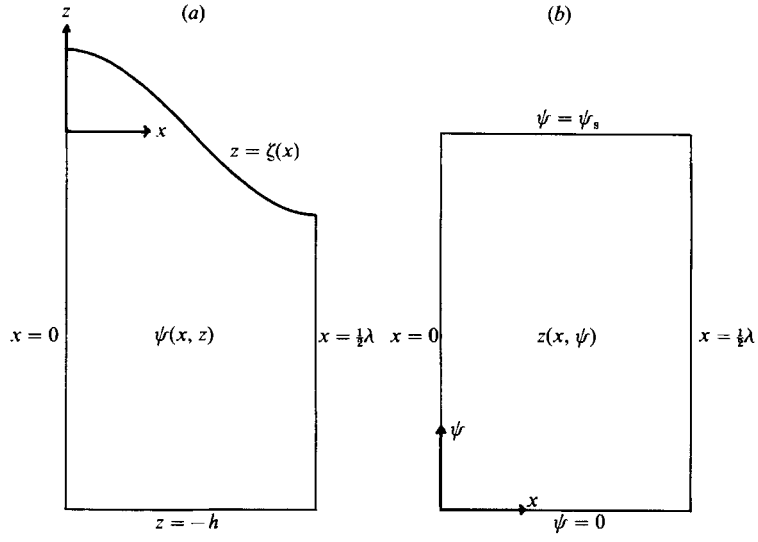

FIGURE 2. The wave domain before and after the Dubreil-Jacotin transformation, (*a*) in original coordinates (x, z), (*b*) in transformed coordinates (x, ψ).

rectangular in geometry and is bounded at the top and bottom by lines of constant ψ. For convenience, the bottom $z = -h$ is chosen to correspond to $\psi = 0$ and the surface streamline is then denoted by the unknown constant value ψ_s.

This rectangular domain in the (x, ψ)-plane is clearly more amenable to numerical computation and in particular to the finite-difference technique. Furthermore the vorticity is now a function of the independent variable ψ. However, this apparent simplification in formulation is only achieved by an increase in algebraic complexity.

The expressions for the local velocity field $(u-c, w)$ from (2.3) become

$$u-c = -\frac{1}{z_\psi}, \quad w = -\frac{z_x}{z_\psi}. \tag{2.8}$$

The analogous form of the Poisson equation (2.4) is

$$z_{xx} z_\psi^2 - 2z_x z_\psi z_{\psi x} + (1+z_x^2) z_{\psi\psi} = \Omega(\psi) z_\psi^3, \tag{2.9}$$

which is a nonlinear equation and valid for $-\infty < x < \infty, 0 \leqslant \psi \leqslant \psi_s$.

The bottom boundary condition (2.3) is that $w = 0$. From (2.8) this implies that either $z_x = 0$ or $z_\psi \to \infty$ on the lower boundary. The latter possibility suggests that $u \to c$, from (2.8), and this cannot be generally true. Thus $z_x = 0$ is the appropriate bottom boundary condition. However, the bottom $z = -h$ is equivalent to $\psi = 0$ and hence the condition can be written simply as

$$z(x, 0) = -h. \tag{2.10}$$

The kinematic free-surface condition (2.6) is automatically satisfied by the transformation. To transform the dynamic free-surface condition note that the free-surface elevation $z = \zeta(x)$ corresponds to $z = z(x, \psi_s)$. Thus (2.7), after use of (2.8), becomes

$$\frac{1}{2z_\psi^2}[1+z_x^2] + gz(x, \psi_s) = \text{constant} \quad \text{on} \quad \psi = \psi_s. \tag{2.11}$$

Solutions of the system (2.9)–(2.11) are to be sought subject to the periodicity

condition and the condition that the mean free-surface position is zero. For practical purposes it is more convenient to use non-dimensional variables. Define X, Ψ, Z and $F(\Psi)$ as follows:

$$X = kx, \quad \Psi = \frac{\psi}{\psi_s}, \quad Z = \frac{z}{h}, \quad F(\Psi) = \frac{h^2}{\psi_s}\Omega(\psi).$$

The non-dimensional forms of (2.8)–(2.11) are

$$u - c = -\frac{\psi_s}{h}\frac{1}{Z_\Psi}, \quad w = -k\psi_s \frac{Z_X}{Z_\Psi}, \tag{2.12}$$

$$Z_{XX}Z_\Psi^2 - 2Z_X Z_\Psi Z_{\Psi X} + \left[\frac{1}{(kh)^2} + Z_X^2\right] Z_{\Psi\Psi} = Z_\Psi^3 \frac{F(\Psi)}{(kh)^2}, \quad -\infty < X < \infty, 0 \leqslant \Psi \leqslant 1, \tag{2.13}$$

$$Z(X, 0) = -1, \tag{2.14}$$

$$Q = Z(X, 1) + \frac{\psi_s^2}{2gh^3}[1 + (kh)^2 Z_X^2]\frac{1}{Z_\Psi^2} \quad \text{on} \quad \Psi = 1, \tag{2.15}$$

where Q is an unknown constant.

The formulation is not yet complete. For given input data $a, \omega, h, U(z)$ the system (2.12)–(2.15) is to be solved to yield the velocity field, surface elevation and the wavelength. The wavelength requires the wavenumber k, the surface elevation is given by $Z(X, 1)$ and the velocity field, from (2.12) requires $Z(X, \Psi)$ in addition to k. All this assumes that ψ_s and $F(\Psi)$ are known. Before a solution can be sought, it is clear that the relationship between ψ_s, $F(\Psi)$, $Z(X, 1)$ and the input data must be established.

Dalrymple (1973, 1977) gives two examples of finite-amplitude wave–current interactions using this formulation. In the first example the vorticity was constant, i.e. $F(\Psi)$ = constant, and in the second the vorticity $F(\Psi)$ was proportional to $\Psi^{-\frac{6}{7}}$. For the first case the wave field is irrotational and the value of ψ_s was obtained using a stream-function model and then treated as an input parameter; the same value of ψ_s was then used for the second example. Although these examples provide an insight into the physical processes and the importance of vorticity, for a general flow specified by $U(z)$ a more fundamental approach is required.

3. Some streamline properties

3.1. *The surface streamline* ψ_s

In the original reference frame the mean horizontal mass flux M, per wave cycle and per unit crest width, in the direction of wave propagation is defined by

$$M = \frac{\omega}{2\pi}\int_0^{2\pi/\omega}\int_{-h}^{\eta(x,t)} u(x, z, t)\,\mathrm{d}z\,\mathrm{d}t, \tag{3.1}$$

which is independent of x.

If the representation for $u(x, z, t)$ given by (2.1) and (2.2) for $-h \leqslant z \leqslant z_t$ is substituted into (3.1), then the expression for M becomes

$$M = \int_{-h}^{z_t} U(z)\,\mathrm{d}z + \frac{\omega}{2\pi}\int_0^{2\pi/\omega}\int_{z_t}^{\eta(x,t)} u(x, z, t)\,\mathrm{d}z\,\mathrm{d}t. \tag{3.2}$$

The first term represents the mass flux beneath the wave due entirely to the current;

the second is the mass flux due to the wave and current between the wave trough and wave crest. This latter quantity cannot in general be determined analytically for waves on a rotational flow. To simplify the form for M in (3.2) introduce the parameter α, defined by

$$\alpha h = \frac{\omega}{2\pi}\int_0^{2\pi/\omega}\int_{z_t}^{\eta(x,t)} u(x,z,t)\,\mathrm{d}z\,\mathrm{d}t, \tag{3.3}$$

so that the mass flux M in (3.2) can be written simply as

$$M = \int_{-h}^{z_t} U(z)\,\mathrm{d}z + \alpha h.$$

In the moving reference frame in which the wave is stationary, the corresponding mean horizontal mass flux M_ψ will be just $M - ch$, i.e.

$$M_\psi = \int_{-h}^{z_t} U(z)\,\mathrm{d}z + \alpha h - ch. \tag{3.4}$$

The stream function $\psi(x,z)$ which is related to the velocity components via (2.3) is defined by the integral representation

$$\psi(x,z) = \int_{(0,-h)}^{(x,z)} [w\,\mathrm{d}x - (u-c)\,\mathrm{d}z], \tag{3.5}$$

which is independent of the path and satisfies the criterion that $\psi(x,-h) = 0$. By choosing a path from $(0,-h)$ to $(x,-h)$ and $(x,-h)$ to (x,z) along straight subpaths, use of the boundary condition $w = 0$ on $z = -h$ combined with (3.5) gives

$$\psi(x,z) = \int_{(x,-h)}^{(x,z)} (c-u)\,\mathrm{d}z = c(z+h) - \int_{-h}^{z} u\,\mathrm{d}z. \tag{3.6}$$

In particular, for points on the free surface, $z = \zeta(x)$ and $\psi(x,\zeta(x)) = \psi_s$, it gives

$$\psi_s = \psi(x,\zeta(x)) = c(\zeta(x)+h) - \int_{-h}^{\zeta} u\,\mathrm{d}z. \tag{3.7}$$

From the definition (3.6), $\psi(x,\zeta(x))$ is seen to represent the instantaneous horizontal mass flux under the wave, per unit crest width, across a plane $x =$ constant. This is measured as positive in the direction of x decreasing. But $\psi(x, \zeta(x)) = \psi_s$ and this is independent of x. Hence the instantaneous mass flux is the same for all values of x and must be equal to the mean mass flux, i.e.

$$\psi_s = -M_\psi,$$

where the minus sign is necessary because ψ_s and M_ψ are measured as positive in opposite directions. With M_ψ given by (3.4), ψ_s becomes

$$\psi_s = (c-\alpha)h - \int_{-h}^{z_t} U(z)\,\mathrm{d}z. \tag{3.8}$$

This is the appropriate form for ψ_s and depends upon an unknown parameter α, the wavenumber k (via $c = \omega/k$) and the position of the wave trough z_t.

If ψ_s in (3.7) and (3.8) are equated, then it is easily shown that

$$\alpha h + c\zeta = \int_{-h}^{\zeta(x)} u\,\mathrm{d}z - \int_{-h}^{z_t} U(z)\,\mathrm{d}z$$

and at $\zeta(x) = z_t$, i.e. the wave trough,

$$\alpha h + cz_t = \int_{-h}^{z_t} (u - U)\,\mathrm{d}z. \tag{3.9}$$

In the moving reference frame, for z in the range $-h \leqslant z \leqslant z_t$, the horizontal velocity field can be written in the appropriate representation of (2.1) and (2.2), i.e.

$$u = U(z) + \sum_{n=1}^{\infty} u_n(z) \cos nkx \tag{3.10}$$

with the origin chosen to be vertically below a wave crest. The wave trough corresponds to the point $(\pi/k, z_t)$ and substitution from (3.10) into (3.9) yields

$$\alpha h + cz_t = \sum_{n=1}^{\infty} (-1)^n \int_{-h}^{z_t} u_n(z)\,\mathrm{d}z. \tag{3.11}$$

If $\psi_n(z)$ is defined by

$$\psi_n(z) = -\int_{-h}^{z} u_n(z)\,\mathrm{d}z, \quad -h \leqslant z \leqslant z_t, \tag{3.12}$$

an alternative form of (3.11) is

$$\alpha h + cz_t = -\sum_{n=1}^{\infty} (-1)^n \psi_n(z_t). \tag{3.13}$$

This relationship will prove useful in examining the vorticity distribution in §4.

3.2. *The relationship between $\psi(x, z)$ and $U(z)$*

Consider the general point (x, z) with $-h \leqslant z \leqslant z_t$. At this point the stream function $\psi(x, z)$ is given by (3.6). On substitution from (3.10) and (3.12) into (3.6) the stream function becomes

$$\psi(x, z) = c(z + h) - \int_{-h}^{z} U(z)\,\mathrm{d}z + \sum_{n=1}^{\infty} \psi_n(z) \cos nkx. \tag{3.14}$$

Now let z take the fixed value z_0. From (3.14), the stream-function variation across the plane $z = z_0$ will be a function of x alone. The mean value of $\psi(x, z_0)$, with respect to x, will be

$$\overline{\psi(x, z_0)}^{x} = c(z_0 + h) - \int_{-h}^{z_0} U(z)\,\mathrm{d}z.$$

Thus there must be a point x_0 in the range $0 \leqslant x_0 \leqslant \pi/k$, i.e. within the half-wavelength domain being used, dependent upon z_0 such that

$$\psi(x_0(z_0), z_0) = c(z_0 + h) - \int_{-h}^{z_0} U(z)\,\mathrm{d}z. \tag{3.15}$$

As the streamlines do not cross this is the only such point within the range of x for a given value of z_0. The equation of the streamline which passes through (x_0, z_0) is

$$c(z + h) - \int_{-h}^{z} U(z)\,\mathrm{d}z + \sum_{n=1}^{\infty} \psi_n(z) \cos nkx = c(z_0 + h) - \int_{-h}^{z_0} U(x)\,\mathrm{d}z$$

and at (x_0, z_0)

$$\sum_{n=1}^{\infty} \psi_n(z_0) \cos nkx_0 = 0. \tag{3.16}$$

Note that in the linear wave theory x_0 would occur for all z_0 at the point $x_0 = \pi/2k$.

This will not be true for a nonlinear wave regime; generally the value of x_0 will be less than $\pi/2k$ but will depend upon z_0. The dependence upon z_0 cannot be easily determined because the functions $\psi_n(z)$ in (3.16) are not known. The importance of this streamline is that it establishes a relationship between the stream function ψ and the input data function $U(z)$.

Not all streamlines can be expressed in the form (3.15); this restriction is limited to the range $0 \leqslant \psi \leqslant \psi(x_0(z_t), z_t)$. For the streamlines $\psi(x_0(z_t), z_t) < \psi \leqslant \psi_s$ there is no simple relation between ψ and $U(z)$. However, ψ_s is given by (3.8) and it is easily shown that if $c \gg U$ then $(\psi_s - \psi(x_0(z_t), z_t)/\psi_s$ is of the same order of magnitude as z_t/h. Thus within the range $0 \leqslant \psi/\psi_s \leqslant 1$, the domain over which ψ/ψ_s is not known will generally be small.

4. The vorticity distribution

The vorticity is known to be constant along a streamline and the vorticity and stream function are related via the Poisson equation (2.4),

$$\Omega = -\nabla^2\psi.$$

At a general point (x, z) the stream function $\psi(x, z)$ is defined by (3.6). Combining these two relations gives the vorticity distribution Ω in terms of the horizontal component of velocity u,

$$\Omega = \frac{\partial u}{\partial z} + \int_{-h}^{z} \frac{\partial^2 u}{\partial x^2} \mathrm{d}z, \tag{4.1}$$

which is valid throughout the wave domain.

Imposing the restriction that z lies within the range $-h \leqslant z \leqslant z_t$ allows simplification of (4.1). Substitution for u from (3.10) and (3.12) yields

$$\Omega = U'(z) - \sum_{n=1}^{\infty} [\psi_n'' - (nk)^2 \psi_n] \cos nkx, \tag{4.2}$$

where a prime indicates differentiation with respect to z. This limitation on the range of z is not severe, since all streamlines must at least touch the domain $-h \leqslant z \leqslant z_t$.

The objective is to determine the vorticity along each streamline. It is convenient to consider the bottom streamline $\psi = 0$, the intermediate streamlines $0 < \psi < \psi_s$ and the surface streamline $\psi = \psi_s$ separately.

4.1. *The bottom streamline* $\psi = 0$

The horizontal bottom boundary $z = -h$ is coincident with the steamline $\psi = 0$. Thus the expression for Ω in (4.2) must be independent of x. Hence the vorticity on the streamline $\psi = 0$ is

$$\Omega(0) = U'(-h). \tag{4.3}$$

4.2. *The intermediate streamlines* $0 < \psi < \psi_s$

In Appendix A, the functions $\psi_n(z), n = 1, 2, \ldots$, are shown to satisfy the inhomogeneous Rayleigh equation

$$\psi_n'' - \left[\frac{U''}{U-c} + (nk)^2\right]\psi_n = g_n(z), \tag{4.4}$$

where $g_n(z)$ is a complicated function of $\psi_1, \ldots, \psi_{n-1}$. The derivation of (4.4) does not assume any properties of the $\psi_n(z)$ other than that the harmonic series (3.10)

converges. However, analytic solutions of this equation cannot be obtained except for the special case in which $U'' = 0$, corresponding to constant vorticity and an irrotational wave motion.

If (4.2) is combined with (4.4) the vorticity distribution becomes

$$\Omega = U'(z) - G(x,z) - \frac{U''}{U-c} \sum_{n=1}^{\infty} \psi_n(z) \cos nkx, \tag{4.5}$$

where

$$G(x,z) = \sum_{n=1}^{\infty} g_n(z) \cos nkx.$$

Now consider the streamline which passes through the point $(x_0(z_0), z_0)$ for z_0 within the range $-h \leqslant z_0 \leqslant z_t$. The value of ψ along this streamline is given by (3.15) and the point $(x_0(z_0), z_0)$ is defined by the property (3.16). On this streamline the vorticity distribution (4.5) is

$$\Omega(\psi) = U'(z_0) - G(x_0, z_0), \tag{4.6}$$

for ψ given by

$$\psi = c(z_0 + h) - \int_{-h}^{z_0} U(z)\, dz.$$

An exact form for $G(x_0, z_0)$ in (4.6) cannot be deduced. However, an approximate form can be obtained if perturbation series solutions to the system of equations (4.4) are sought. If ϵ is a small parameter for the flow, such as the wave slope, a series solution in powers of ϵ for each $\psi_n(z)$ and $g_n(z)$ can be constructed; the formulation and details are contained in Appendix B. The extension of this procedure to the series $G(x_0, z_0)$ is outlined in Appendix C and the result is

$$G(x_0, z_0) = \frac{\psi_1^2(z_0)}{4(U-c)} \left[\frac{U''}{U-c}\right]' \Big|_{z=z_0} + O(\epsilon^4).$$

Substitution into (4.6) gives the vorticity distribution – streamline relation

$$\Omega(\psi) = U'(z_0) - \frac{\psi_1^2(z_0)}{4(U-c)} \left[\frac{U''}{U-c}\right]' \Big|_{z=z_0} + O(\epsilon^4), \tag{4.7}$$

on

$$\psi = c(z_0 + h) - \int_{-h}^{z_0} U(z)\, dz.$$

The vorticity distribution in (4.7) is of an interesting form. There is a known mean flow contribution of zero order, a second-order correction term and subsequent correction terms being at most of fourth order. To use a finite-amplitude wave theory the second-order correction term must be included though the first-order stream function $\psi_1(z)$ is unknown. This second-order term depends essentially upon $\psi_1(z)$ and the derivatives of $U(z)$, since generally the $U-c$ contribution will be dominated by the c factor. As $\psi_1(z)$ represents the mass flux under the first-order wave solution, $\psi_1(z)$ will increase with z and be largest near the free surface. The $U(z)$ derivative contributions will be most significant whenever $U(z)$ changes rapidly. Thus the combined influence of $\psi_1(z)$ and $U(z)$ is likely to be strongest close to the free surface and in the vicinity of strong shear layers in the flow.

To obtain a usable approximation for $\psi_1(z)$, note that the equation (4.4) for $\psi_1(z)$ together with the results of Appendix B gives

$$\psi_1'' - \left[\frac{U''}{U-c} + k^2\right] \psi_1 = O(\epsilon^3).$$

From (3.12), $\psi_1(-h) = 0$. Further, from (3.13), $\psi_1(z_t) = \alpha h + cz_t + O(\epsilon^2)$. Thus to determine $\psi_1(z)$ solutions are sought of the system

$$\left.\begin{aligned} \psi_1'' - \left[\frac{U''}{U-c} + k^2\right]\psi_1 = 0, \\ \psi_1(-h) = 0, \quad \psi_1(z_t) = \alpha h + cz_t. \end{aligned}\right\} \tag{4.8}$$

This will reduce the error term in (4.7) to $O(\epsilon^3)$, but the system (4.8) is readily solved numerically as an initial-value problem and the method used by Thomas (1981) is applicable.

4.3. *The surface streamline* ψ_s

The surface streamline touches the domain $-h \leqslant z \leqslant z_t$ at the point $(\pi/k, z_t)$, corresponding to the wave trough. Thus the vorticity on the surface streamline can be obtained using the expression (4.5) evaluated at $(\pi/k, z_t)$,

$$\Omega(\psi_s) = U'(z_t) - \sum_{n=1}^{\infty} (-1)^n g_n(z_t) + \frac{U''}{U-c} \sum_{n=1}^{\infty} (-1)^n \psi_n(z_t).$$

The last term can be simplified using (3.13) and, on rearrangement,

$$\Omega(\psi_s) = U'(z_t) + (\alpha h + cz_t)\frac{U''}{U-c}\bigg|_{z=z_t} + \sum_{n=1}^{\infty} (-1)^{n+1} g_n(z_t). \tag{4.9}$$

The series in (4.9) is considered in Appendix D and its form is determined to give an error term of $o(\epsilon^4)$. However, the form is very complicated and not amenable to algebraic manipulation or numerical evaluation. If one order of magnitude of accuracy is sacrificed then the following simple expression is obtained:

$$\sum_{n=1}^{\infty} (-1)^{n+1} g_n(z_t) = \tfrac{1}{4}(\alpha h + cz_t)^2 \left\{\frac{1}{U-c}\left[\frac{U''}{U-c}\right]'\right\}_{z=z_t} + O(\epsilon^3). \tag{4.10}$$

A parallel with irrotational wave theory suggests that the error is of $O(\epsilon^4)$ but this is not easily proved, nor required, since the vorticity distribution for a general streamline using (4.7) and (4.8) contains an error $O(\epsilon^3)$. Combining (4.9) and (4.10) gives the surface vorticity distribution finally as

$$\Omega(\psi_s) = U'(z_t) + (\alpha h + cz_t)\frac{U''}{U-c}\bigg|_{z=z_t} + \tfrac{1}{4}(\alpha h + cz_t)^2 \left\{\frac{1}{U-c}\left[\frac{U''}{U-c}\right]'\right\}_{z=z_t} + O(\epsilon^3). \tag{4.11}$$

This expression appears to be a power series in $(\alpha h + cz_t)$, but it cannot be readily extended to include higher powers. However, the importance of strong shear layers near to the free surface is apparent in the higher-order terms and consistent with the nonlinear effects for the intermediate streamlines, as described by (4.7).

The vorticity–streamline distribution is now determined via (4.3), (4.7) and (4.11), noting that (4.8) is required for evaluation of (4.7). On streamlines for which $\psi(x_0(z_t), z_t) < \psi < \psi_s$, the value of $\Omega(\psi)$ can be obtained by numerical interpolation.

If the waves are small then an approximation consistent with the linear wave

theory can be introduced. This requires the vorticity–stream function relationship to be given by terms up to and including those of $O(\epsilon)$ in (4.3), (4.7) and (4.11), i.e.

$$\begin{aligned} \Omega(\psi) &= U'(-h), && \psi = 0 \\ &= U'(z_0), && \psi = c(z_0+h) - \int_{-h}^{z_0} U(z)\,\mathrm{d}z \\ &= U'(z_t) + (\alpha h + cz_t)\frac{U''}{U-c}\bigg|_{z=z_t}, && \psi = \psi_s. \end{aligned} \tag{4.12}$$

For many current profiles, which do not contain regions where $U''(z)$ or the higher derivatives are large, the relatively simple expression (4.12) is likely to provide an adequate vorticity–stream function relationship.

5. Numerical considerations

5.1. *Input data*

The input data are usually given as the wave amplitude a, radian frequency ω, mean water depth h and mean flow profile $U(z)$ below the wave trough. Alternatives to the first two are the wave height H and period T respectively.

In practice the input parameters a, ω, h are given either by specification or from experimental data. The input mean profile $U(z)$ will have a functional representation only if the profile is of a specified analytic form and in such a case the derivatives of $U(z)$ can usually be readily obtained. If experimental measurements are the source of the input data then $U(z)$ will be defined by the set of values $\{U(z_i), i = 1, \ldots, N_z\}$ and the requirement is a numerical procedure that will provide values for $U(z)$ and its derivatives as the need arises. The comparison between theory and experiment presented in §8 has a discrete set of experimentally obtained values to define the function $U(z)$ and it is clearly important that this discrete data set is carefully handled.

The task of determining a numerical representation for $U(z)$ throughout the range $-h \leqslant z \leqslant z_t$ is composed of two main parts. First as $U(-h)$ and $U(z_t)$ will not usually be measured, there is the difficulty of extrapolation below the first and above the last data points to obtain estimates for $U(-h)$ and $U(z_t)$. Secondly, suitable interpolation techniques must be employed to determine $U(z)$ and its first two derivatives for the range $-h \leqslant z \leqslant z_t$ for some given value of z_t. The extrapolation problem is clearly easier if the first and last data points are as close to $z = -h$ and $z = z_t$ as possible. Reasonable estimates for $U(-h)$ and $U(z_t)$ can be obtained using rational polynomial approximation with an appropriate number of adjacent data points. An alternative method for $U(-h)$ is to use a logarithmic profile near the bed and fit this to the nearest two data points; the estimate for $U(-h)$ is the value predicted for the upper edge of the laminar sublayer. The estimates obtained for $U(-h)$ and $U(z_t)$ at this stage are regarded as good initial guesses for the interpolation problem.

The essential requirement of the interpolation process is that it supplies values for $U(z)$ and its first two derivatives at all points within the range $-h \leqslant z \leqslant z_t$ when the input data are the experimental data set $\{U(z), i = 1, \ldots, N_z\}$ together with the estimates obtained for $U(-h)$ and $U(z_t)$. Additionally it is usually necessary to incorporate a small degree of smoothing to counterbalance experimental errors in measurement. If the experimental data points are each given equal weighting, with correspondingly smaller weighting given to the initial estimates for $U(-h)$ and $U(z_t)$,

then the implementation of a standard interpolation routine with smoothing will usually work well. The method used here was a weighted least-squares fit using orthogonal polynomials. Cubic spline interpolation could also be used but this has two drawbacks, both of which concern the evaluation of the second derivative $U''(z)$. The first is associated with the nature of spline interpolation: between any two data points the spline is a cubic and hence the second derivative is a linear function of z and this may be a poor approximation in regions of high rate of shear. Secondly, many smoothing routines involving cubic splines minimize a weighted average of the modulus of the second derivative over the domain $-h \leqslant z \leqslant z_t$; this is clearly an undesirable feature if the second derivative is most important when its magnitude is greatest.

5.2. *The unknown parameters*

The unknown quantities which appear in the formulation of §§3 and 4 are the wavenumber k, the wave-like mass flux α and the position of the wave trough z_t. In addition the general position of the free surface is also unknown and the wave trough is just the lowest point of the free surface. The method of solution employed must therefore determine the parameters α and k, together with a functional representation of the free surface.

The free surface is described by $z = \zeta(x)$ or alternatively by $z = z(x, \psi_s)$ depending upon the frame of reference and independent variables being used. There are three conditions to be imposed upon $\zeta(x)$: the free surface must be periodic, the mean value of $\zeta(x)$ over a wavelength must be zero and the amplitude of the first harmonic of $\zeta(x)$ must be the input parameter a. Each of these conditions can be treated as a constraint in an optimization process. However, for the present purposes it is easier to use a trigonometric polynomial of order N to approximate the function $\zeta(x)$:

$$\zeta(x) = \sum_{n=1}^{N} a_n \cos nkx, \quad a_1 = a, \tag{5.1}$$

which can alternatively be written as

$$Z(X, 1) = \sum_{n=1}^{N} \frac{a_n}{h} \cos nX. \tag{5.2}$$

The form for the free surface satisfies all of the necessary conditions, although the constants $a_n, n = 2, \ldots, N$ are unknown.

The representation (5.1) of the surface elevation can be regarded as analogous to that used for Stokes waves and thus is best suited to waves on water of finite depth, i.e. kh of $O(1)$. For shallow water the number of harmonics required will increase as kh decreases and accordingly the form (5.1) may not be the most appropriate one to use. In such cases a constraint formulation may be better.

For a specified value of N, there are $N+1$ unknown parameters to be determined; these are $k, \alpha, a_2, \ldots, a_N$.

5.3. *Optimization strategy*

For specified values of the parameters $k, \alpha, a_1, \ldots, a_N$ a solution of the governing equation (2.13) is sought over the range of half a wavelength, i.e.

$$Z_{XX} Z_\Psi^2 - 2Z_X Z_\Psi Z_{\Psi X} + \left[\frac{1}{(kh)^2} + Z_X^2\right] Z_{\Psi\Psi} = Z_\Psi^3 \frac{F(\Psi)}{(kh)^2}, \quad 0 \leqslant X \leqslant \pi, 0 \leqslant \Psi \leqslant 1. \tag{5.3}$$

The boundary conditions imposed on the lower and upper boundaries are given by (2.14) and (5.2) respectively,

$$Z(X,0) = -1, \quad Z(X,1) = \sum_{n=1}^{N} \frac{a_n}{h} \cos nx \tag{5.4}$$

and periodicity constraints are imposed on the side boundaries $X = 0, \pi$.

The non-dimensional vorticity distribution $F(\Psi)$ in (5.3) is defined to be $h^2\Omega(\psi)/\psi_s$ from (2.11) and the appropriate $\Omega(\psi) - \psi$ relationship is given in §4. As both $\Omega(\psi)$ and ψ_s depend upon α, k and z_t, the function $F(\psi)$ will also vary with α, k and z_t. If $\boldsymbol{y}$ is the $(N+1)$-dimensional vector with components $(k, \alpha, a_2, \ldots, a_N)$, then $\boldsymbol{y}$ describes the unknown parameters and for given $\boldsymbol{y}$ the function $F(\Psi)$ is regarded as known.

The boundary-value problem defined by (5.3) and (5.4) is well-posed and it is assumed that solution function $Z(X, \Psi)$ can be obtained. For a general value $\boldsymbol{y}$ the condition that the free surface is a surface of constant pressure will not be satisfied and the function on the right-hand side of (2.15) will be a function of X. Define the function $q(X;\boldsymbol{y})$ by

$$q(X;\boldsymbol{y}) = Z(X,1) + \frac{\psi_s^2}{2gh^3}[1 + (kh)^2 Z_X^2]\frac{1}{Z_\Psi^2} \quad \text{on} \quad \Psi = 1.$$

If $q(X;\boldsymbol{y})$ is independent of X then the free surface will be of constant pressure.

To gain an estimate of the error to the free-surface boundary condition, define $\bar{q}(\boldsymbol{y})$ to be the mean value of $q(X;\boldsymbol{y})$ over one half-wavelength,

$$\bar{q}(\boldsymbol{y}) = \frac{1}{\pi}\int_0^\pi q(X;\boldsymbol{y})\,\mathrm{d}X$$

and define the root-mean-square error $R(\boldsymbol{y})$ to be

$$R(\boldsymbol{y}) = \left[\frac{1}{\pi}\int_0^\pi [q(x;\boldsymbol{y}) - \bar{q}(\boldsymbol{y})]^2\,\mathrm{d}x\right]^{\frac{1}{2}}. \tag{5.5}$$

If $R(\boldsymbol{y}) = 0$ then the free-surface condition will be satisfied identically. Thus the requirement may seem to be to determine $\boldsymbol{y}$ so that $R(\boldsymbol{y}) = 0$. As $R(\boldsymbol{y}) \geqslant 0$, this is a minimization problem in the $N+1$-dimensions defined by the components of $\boldsymbol{y}$. In practice (5.3) must be solved numerically and the solution will contain numerical errors, hence the theoretical minimum of $R(\boldsymbol{y}) = 0$ will not usually be attainable.

However, it is not sufficient just to obtain a value of $\boldsymbol{y}$ which minimizes $R(\boldsymbol{y})$. Although the vorticity–streamline relationships from §§3 and 4 are given in terms of the input data, they also contain a dependence upon the components of $\boldsymbol{y}$. This dependence on $\boldsymbol{y}$ cannot be arbitrary because there must be compatibility with the original input data, i.e. the value of $\boldsymbol{y}$ which minimizes $R(\boldsymbol{y})$ must be consistent with the chosen reference frame. A compatibility condition is established as follows.

For a given value of $\boldsymbol{y}$ and a solution function $Z(X, \Psi)$, the horizontal component of velocity in the moving reference frame will be given by (2.12), i.e. $u(x,z) = c - \psi_s/(hZ_\Psi)$. If z is in the range $-h \leqslant z \leqslant z_t$, the mean value of u over half a wavelength will be

$$\bar{u}(z;\boldsymbol{y}) = \frac{k}{\pi}\int_0^{\pi/k} u(x,z)\,\mathrm{d}x.$$

The input data for the mean flow are given as the data set $\{U(z_i), i = 1, \ldots, N_z\}$. Thus the output velocity field is compatible with the input data when condition (2.1) is satisfied, i.e.

$$\bar{u}(z_i;\boldsymbol{y}) = U(z_i)$$

for $i = 1, \ldots, N_Z$. A global condition is preferable to N_Z individual conditions and is obtained by defining $\sigma(y)$ to be the mean-square non-dimensional velocity error given by

$$\sigma(y) = \frac{1}{N_z gh} \sum_{n=1}^{N_z} [\bar{u}(z_i; y) - U(z_i)]^2. \tag{5.6}$$

All of the individual conditions will be satisfied identically if and only if $\sigma(y) = 0$. If the input mean flow is given by an analytic function rather than a discrete data set, an integral equivalent of (5.6) is necessary.

An appropriate strategy is to minimize $R(y)$ subject to the equality constraint $\sigma(y) = 0$. However, numerical considerations suggest that $\sigma(y) = 0$ cannot be attained exactly and the algorithm must take account of this. It may seem that the best approach would be to minimize $R(y)$ subject to the inequality constraint $\sigma(y) < u_c$, where u_c is a prescribed acceptable mean velocity error, but there are two good reasons for not adopting this procedure. First, finding an attainable realistic value for u_c is not easy and secondly the requirement is to make $\sigma(y)$ as small as possible, not just $\sigma(y) < u_c$. A better approach is to proceed with the equality constraint and be aware of the numerical difficulties associated with $\sigma(y)$.

Following Greig (1980) a minimum is sought of the objective function

$$L(y, \gamma) = R(y) - \gamma\sigma(y) + \tfrac{1}{2}W\sigma^2(y), \tag{5.7}$$

where γ is a Lagrange multiplier and W is a weighting factor. The weighting factor W ensures the correct behaviour of $L(y, \gamma)$ with regard to the constraint and can be given arbitrary values; for the present work the value $W = 10$ was used satisfactorily.

The algorithm for obtaining the minimum of (5.7) is composed of three simple steps. (i) Put $\gamma = 0$ and obtain the unconstrained minimum of $L(y; 0)$; this will occur when $y = y_0$, corresponding to a constraint error $\sigma(y_0)$. (ii) Define $\gamma_1 = -W\sigma(y_0)$ and minimize $L(y; \gamma_1)$ to obtain y_1 and $\sigma(y_1)$. (iii) For $i = 2 \ldots$, put $\gamma_i = \gamma_{i-1} - W\sigma(y_{i-1})$ and minimize $L(y; \gamma_i)$ to obtain y_i and $\sigma(y_i)$.

The algorithm is halted when $\sigma(y_i)$ is deemed to be sufficiently small. For almost all of the current profiles studied it was not found necessary to implement step (iii), the value $\sigma(y_1)$ was very close to the best that could be achieved and higher iterations brought little appreciable increase in accuracy. Use of an algorithm such as the one outlined above requires a suitably robust unconstrained minimization routine; this is usually available as a standard computer library routine.

5.4. *Finite-difference solution procedure*

In order to implement the optimization procedure following (5.7), it is necessary to be able to determine the objective error function $R(y)$ and constraint error $\sigma(y)$, defined by (5.5) and (5.6) respectively, for an arbitrary value of y. This requires solution of (5.3) on the given rectangular domain, subject to the fixed boundary conditions (5.4) and the periodicity conditions on $X = 0, \pi$.

The equation (5.3), subject to the prescribed boundary conditions, is solved using a finite-difference scheme. A uniform grid is generated by the incremental measures $\Delta\Psi, \Delta X$ in the Ψ, X-directions respectively and the magnitude of $\Delta\Psi$, ΔX is controlled by the integers M_g, N_g such that

$$\Delta\Psi = \frac{1}{M_g}, \quad \Delta X = \frac{\pi}{N_g}. \tag{5.8}$$

The grid is composed of the points $\{(\Psi_i, X_j); i = 1, \ldots, M_g + 1; j = 1, \ldots, N_g + 3\}$ and

the value of $Z(X_j, \Psi_i)$ is denoted by Z_{ij}. In this notation the bottom and top streamlines correspond to $i = 1$ and $i = M_g + 1$ respectively and the wave crest and trough correspond to $j = 2$ and $j = N_g + 2$. Grid points strictly outside the half-wavelength with $j = 1$ and $j = N_g + 3$, are utilized to implement the periodicity conditions.

For internal grid points, all derivatives in (5.3) can be approximated by central-difference formulae and Z_{ij} expressed as the weighted average of its neighbouring points. The appropriate formula for Z_{ij} is given by Dalrymple (1973, 1977). Note that the boundary points with $i = 1$ or $i = M_g + 1$ are of a fixed value for given y and cannot change during the solution procedure.

At the grid points not corresponding to the top and bottom streamlines, initial values of Z_{ij} are allocated using the linear irrotational wave solutions. The solution is obtained iteratively using successive over-relaxation, with the relaxation parameter taking the value specified by Roache (1982, p. 118) for given M_g and N_g. Convergence was deemed to have been achieved when the maximum error over the whole grid between successive iterations was less than some prescribed value, usually taken to be 10^{-6}. The procedure is similar to that described by Dalrymple (1973, 1977) but is simpler to implement because the boundary condition on the surface streamline is fixed for given y.

Once the values of Z_{ij} have been determined to the required degree of accuracy, then all necessary derivatives can be obtained using either difference formulae or interpolating functions. Hence $R(y)$ and $\sigma(y)$ can be calculated.

5.5. *Implementation*

The first step is to choose the number of harmonics N which are employed to approximate the free surface and to assign initial values of the unknown parameters. In the linear wave regime $N = 1$ can be used, but in general N must be increased as the wave slope increases or the wavelength-to-depth ratio decreases. The wave-number k is assigned a value derived from the linear dispersion relation and this may contain a representative current term if required, e.g. let the initial value k satisfy $(\omega - kU_r)^2 = gk \tanh kh$, where U_r is a mean-current term which represents the input data in some way. An estimate for α can be obtained using a second-order irrotational approximation to (3.9). The higher-order surface harmonics $a_2, \ldots, a_N$ are most easily represented by relations of the type $a_2 = \frac{1}{6}a_1$, $a_3 = \frac{1}{6}a_2$, etc.

The following procedure was found by experience to provide the most suitable way of implementing the numerical model for an arbitrary input set.

With the unknown parameters assigned the initial values given above, the optimization routine is run for two iterations with a 20×40 grid. This provides an estimate for the minimum of $L(y, \gamma)$ with corresponding solution vector y_1, constraint error measure $\sigma(y_1)$ and Lagrange multiplier γ_1. Finally, with the same value for γ_1, the objective $L(y, \gamma_1)$ is minimized, using a 40×60 grid, to obtain updated estimates for $y_1, \sigma(y_1)$ and the solution function $Z(X, \Psi)$. This last step, with a greater number of grid points, essentially provides a fine-tuning mechanism and can be omitted if high-accuracy solutions are not required and $U(z)$ is a sufficiently smooth function. All flow quantities, such as surface profile or velocity field, can then be calculated as necessary.

6. Test procedures

For a given set of input parameters a, ω, h and arbitrary mean flow $U(z)$, no finite-amplitude solutions exist except for the special cases in which either $U(z)$ is constant or possesses a constant derivative. The earlier model of Dalrymple (1973, 1977) requires U to be specified as a function of ψ and so cannot be used directly for comparison. If attention is restricted to the linear waves regime, then the model described by Thomas (1981) can be used to obtain a solution numerically for a mean flow with an arbitrary distribution of vorticity. The present model was tested by comparison with the available results for linear waves when $U(z)$ is arbitrary and with the special cases of either $U(z)$ or $U'(z)$ being constant for finite-amplitude waves. In each case the model was implemented using the procedure outlined in the previous section.

Generally very good agreement was found between the predictions of the present model for wavelength and velocity profiles and those obtained using the Thomas (1981) model in the linear wave regime. Comparisons were made with both analytical forms and experimentally obtained profiles for the mean flow $U(z)$. When the mean flow is prescribed to take a given analytic form, the amplitude a was chosen to ensure that the wave slope was sufficiently small to be well within the linear wave regime; good agreement was obtained with just one harmonic to describe the free surface, i.e. $N = 1$. For the experimental data $N = 3$ was used; this is because the experimental current profiles presented by Thomas for linear waves are measured without waves and the mean flow with the waves may vary slightly owing to second-order effects, though these are likely to be very small. The agreement between the experimental results and present predictions was always at least as good as that found in the earlier study by Thomas (1981).

It should be noted that the current profiles with and without the waves will only be the same in the linear regime. For nonlinear waves this will certainly not be the case, owing to the redistribution of the vorticity in the undisturbed current by the nonlinear interaction processes.

For finite-amplitude waves two comparisons with available results and theories were made. The first was for a constant current on water of finite depth and the second corresponds to a current with constant vorticity within the shallow-water regime.

An input data set of $h = 0.5$ m, $a = 50$ mm, $\omega = 1.6\pi$ rad/s and $U(z) = -0.1$ m/s was selected. These values were chosen because they are of similar magnitudes to the experimental data considered in §8. As the waves are irrotational and of finite amplitude, Stokes' fifth-order theory can be used to determine the wave properties. The appropriate coefficients are given by Skjelbreia & Hendrickson (1960) and the amendment at the fifth order due to Fenton (1985) was incorporated. For the data given, the Stokes theory predicts a wavelength of 2.0379 m and the corresponding value of kh is approximately 1.54 so that the waves are towards the upper end of the finite-depth regime. The numerical model predicts a wavelength of 2.0394 m for a 20×40 grid and 2.0385 for a 40×60 grid and in each case the error measure $R(y_1)$ was $3.5D' - 5$. Not surprisingly, the finer grid produces the better approximation, with an error at the fifth significant figure, as the wave motion will show a considerable variation with depth in this regime. Good agreement was also obtained between the velocity profiles predicted by each model.

The second finite-amplitude data set was $h = 10$ ft, $T = 10$ s, $H = 2$ ft, $U(z) = -0.3(z + 10)$ ft/s. These data were used by Dalrymple (1973, 1977) to generate

Harmonics	Grid size	λ	ψ_s	$R(y_1)$
7	20×40	164.72	178.88	$3.1D'-5$
	40×60	164.70	178.87	$3.5D'-5$
9	20×40	164.71	178.89	$7.0D'-6$
19th-order stream-function theory		164.6	178.76	$5.9D'-6$

TABLE 1. Numerical predictions for the wavelength λ and surface stream function ψ_s for the data set $h = 10$ ft, $T = 10$ s, $H = 2$ ft and $U(z) = -0.3(z+10)$ ft/s. The values obtained by Dalrymple (1973, 1977) using a nineteenth-order stream-function theory are also shown, together with the mean free-surface boundary-condition error

input data for a consistency test in his finite-difference numerical model. The input data required by Dalrymple were the wavelength λ and the surface streamline mass flux ψ_s. A nineteenth-order stream function model, as described by Dalrymple (1973, 1974), produced a highly accurate solution of $\lambda = 164.6$ ft and $\psi_s = 178.76$ ft^2/s and this corresponds to $kh = 0.3817$ which lies within the shallow-water-wave regime. The present model was employed to predict values for λ and ψ_s for comparison with those obtained using the stream function theory; the results are presented in table 1. Predictions are presented for seven and nine harmonics and for two grid sizes. As expected the solutions improve, measured by the criterion that $R(y_1)$ becomes smaller, as the number of harmonics increases. There is a relatively smaller increase in accuracy for a refinement in grid size and this could be anticipated for the shallow-water-wave regime. One interesting feature of the solutions is that the accuracy of the nine harmonic models is of comparable order with that of the high-order stream- function model.

In each of the test procedures described above the numerical model performed very well. However, it should be pointed out that for these special cases the numerical model is very inefficient in comparison with existing models. The strength of the present numerical model is that it will still work well when $U(z)$ is an arbitrary function and the waves are of finite amplitude; the previous models cannot be extended to include such general cases.

7. The experimental facility and procedure

7.1. *Experimental facility*

A detailed description of the experimental facility has previously been given by Thomas (1981). For the present series of experiments one additional feature was included. This was a microprocessor-controlled data analyser which was commissioned to produce an accurate on-line analysis of the velocity signals provided by the laser-Doppler anenometer. For each wave cycle the data analyser determined the maximum, minimum and mean voltages and finally gave the averaged values of these quantities over some specified number of consecutive wave cycles.

7.2. *Experimental procedure*

The following procedure was adopted for each of the experiments.

The pump motor was set to the required speed to generate the recirculatory flow and the water depth adjusted to give the desired value when measured immediately in front of the paddle (which is essentially a region of still water in the absence of waves).

A steady wavetrain was then generated at a prescribed frequency and the amplitude of the waves was controlled by the stroke of the sinusoidal paddle motion. The mean water depth in front of the wavemaker was checked and adjusted if necessary.

The average maximum, minimum and mean horizontal velocities per wave cycle were measured at a number of points, typically twenty, beneath the wave trough. The measuring points were approximately uniformly spaced with the top point being as close as possible to the wave trough. These averaged velocity values were obtained by measuring the appropriate quantity over a number of consecutive wave cycles and determining the average such value; usually 200 cycles were used, with the purpose of eliminating the influence of turbulence in the data. The mean horizontal values describe the current $U(z)$ and the maximum and minimum values correspond to the horizontal velocity field below the wave crest and trough respectively. Vertical velocities were not measured because they do not provide an input to the numerical model and were not deemed necessary for comparison with theoretical predictions. The average maximum horizontal velocity per wave cycle was also measured at some points between the wave trough and crest; this is for comparison with the numerical predictions.

The surface profile was also considered similarly, with the averaged first-harmonic magnitude providing an input to the numerical model. Higher-order harmonics were also measured as they yield insight into both nonlinearity and higher-order flume effects. The water depth h was determined accurately at the measuring site using the mean of the signal from the waveheight recorder. Finally two wave probes were used to determine the wavelength.

8. Results

In the series of experiments described here the water depth immediately in front of the paddle was maintained at 0.55 m. The wave frequency was 0.8 Hz and the same paddle displacement was used to generate the waves in each experiment.

The measured velocities and wavelengths, together with the corresponding theoretical predictions, are presented graphically in figures 3–7 and tabulated in table 2. Figure 3 corresponds to the pump not being in operation and the current within the recirculatory system is generated entirely by the wave motion; the other figures are arranged as a sequence of increasingly adverse pump-generated currents. In each case the input current profile $U(z)$ is defined by the set of circles shown on the figure and the water depth h and amplitude a are given in the table. Velocity profiles predicted by the numerical model are shown in the figures as solid lines and the measured maximum or minimum velocity values are denoted by crosses.

For each current profile the numerical model was implemented in the way described in §6 and the results presented correspond to a 40×60 grid. The quantity $\bar{U}$ is defined to be the mean depth-averaged current below the wave trough and the appropriate value of $\bar{U}$ for each profile is given in table 2. In each implementation of the model the final value of the mean constraint (5.6) was determined; in dimensional terms the error in satisfying the constraint exactly lay between 0.2% and 0.4% of the appropriate value of $\bar{U}$, which is considered to be highly satisfactory. In all cases five surface harmonics, i.e. $N = 5$, were used.

The measured wavelength λ_m and the predicted wavelength λ_p are seen in table 2 to agree very well, with a maximum relative error of 0.5%. From figures 3–7, generally good agreement is seen to exist between the measured velocity profiles

Figure	h	a	U	λ_m	λ_p	λ_{p1}	$\lambda_{\bar{U}}$	λ_L
3	0.551	64.51	14.44	2.288	2.299	2.299	2.330	2.228
4	0.548	68.89	−85.69	2.129	2.127	2.133	2.149	2.030
5	0.549	69.94	−118.01	2.084	2.091	2.087	2.090	1.984
6	0.545	72.42	−166.53	2.008	2.009	1.996	1.999	1.878
7	0.549	75.73	−218.09	1.832	1.841	1.812	1.915	1.662

TABLE 2. The measured and predicted physical properties of the interactions illustrated in figures 3–7. All wavelengths and the mean water depth h are measured in m; wave amplitudes are denoted by a and are measured in mm. The quantity $\bar{U}$, measured in mm/s, is the depth-averaged mean flow below the wave trough. The measured wavelength is λ_m and there are four predicted values: λ_p, λ_{p1} are the predicted values from the numerical model using the full vorticity distribution of §4 and the approximate form of (4.12) respectively, $\lambda_{\bar{U}}$ is the fifth-order Stokes theory value for constant current $\bar{U}$, and λ_L corresponds to the linear model of Thomas (1981)

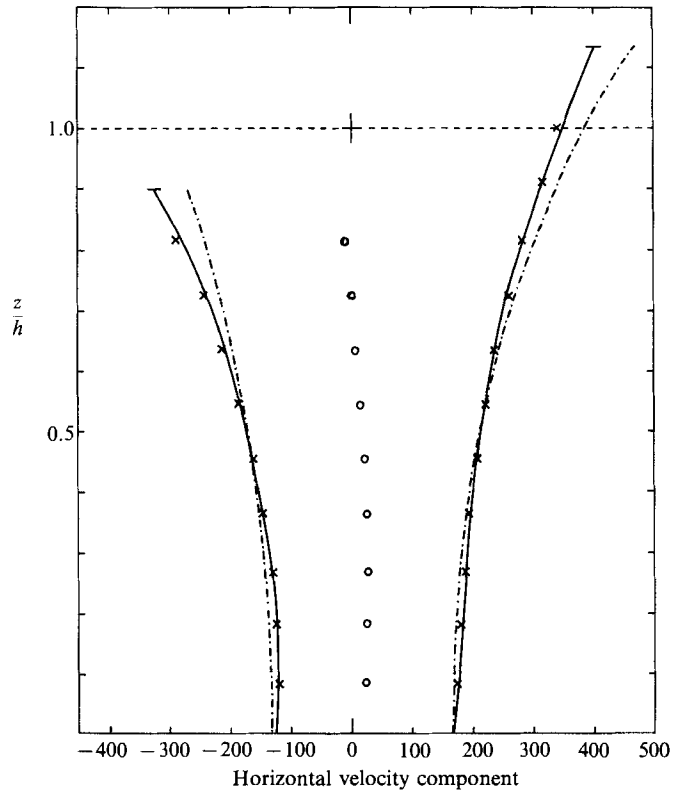

FIGURE 3. Comparison between theory and experiment for the horizontal particle velocities under the wave crest and wave trough. All velocities are measured in mm/s and the physical properties of the system are given in table 2. ○, mean flow (used as input data); ×, measured velocities; ——, predicted profile; —·—, theoretical profile for constant current. For this current, $\bar{U} = 14.44$ mm/s.

under the wave crest and trough and the corresponding theoretical predictions. The region of greatest disparity occurs close to the free surface and is most noticeable under the wave trough in figures 5 and 6 and under the wave crest in figure 7. In each case the disagreement is confined to the streamlines closest to the free surface but the cause of the phenomenon is not readily identified. An important contributory factor

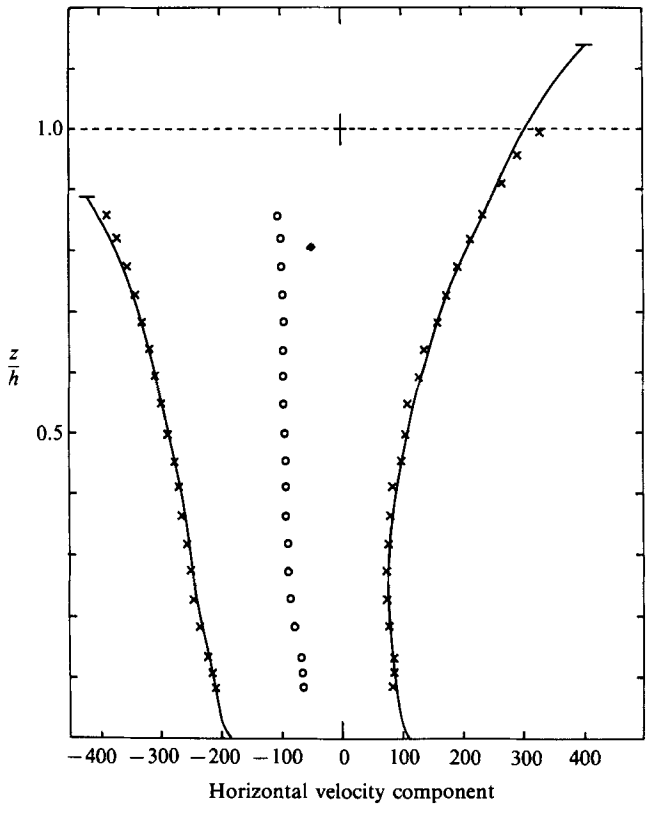

FIGURE 4. As for figure 3, with $\bar{U} = -85.69$ mm/s.

may be the presence of free second and higher harmonics in the wavetrain, and these are indeed noticeable in the harmonic analysis of the surface elevation, but would not seem to be large enough to completely explain the observed difference between theory and experiment.

These free harmonics arise when attempting to generate a wavetrain of finite amplitude using a sinusoidal paddle motion; the phenomenon is described by Hansen & Svendsen (1974). Reflections from the beach or the screens (which were not found to appreciably change the beach reflection coefficient) are unlikely to be contributory factors to the disparity because the area of disagreement is confined to close to the free surface. With these minor disagreements acknowledged the numerical model can be regarded as predicting wavelengths and velocity profiles with a good degree of accuracy.

The present numerical model is applicable to waves of finite amplitude on a current containing an arbitrary distribution of vorticity. At this point, it is useful to use existing theories and the experimental results to determine the influence of both the finite-amplitude character of the waves and the vorticity.

To assess the importance of finite amplitude the wavelength prediction using the linear theory for an arbitrary distribution of vorticity was calculated for each current profile. The quantity appears in table 2 as λ_L and the method of calculation is given by Thomas (1981). From table 2 the maximum relative error between λ_m and λ_L occurs for the maximum adverse current and is approximately 10%. Although the other profiles do not exhibit as large a disparity it is clear that finite-amplitude

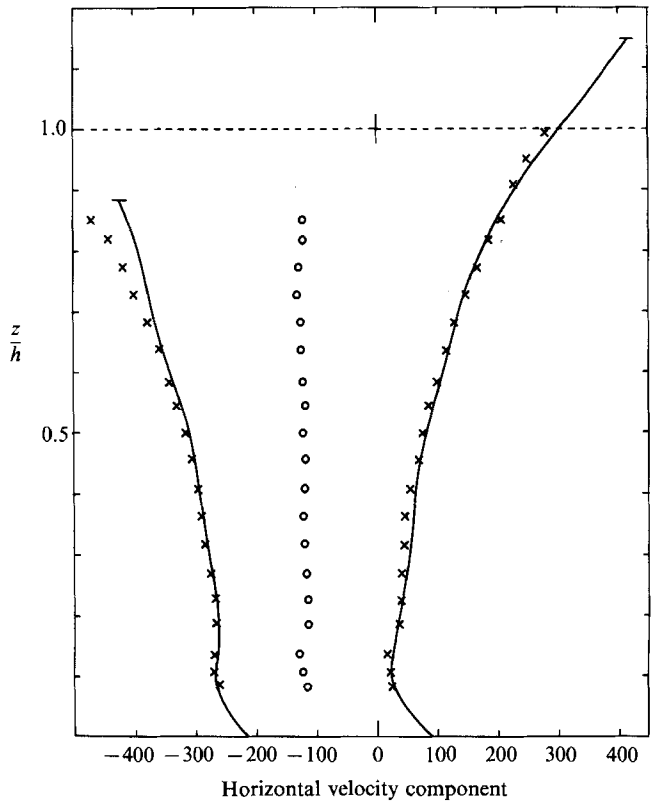

FIGURE 5. As for figure 3, with $\bar{U} = -118.01$ mm/s. Where appropriate in figures 5–7 the velocity prediction using the first-order vorticity distribution, described by (4.12), is denoted by ....

effects are very significant and this is confirmed by a comparison of the velocity profile predictions, although these profiles are not presented here.

For a constant current $\bar{U}$ the wavelength calculated using the Stokes fifth-order wave theory is denoted in table 2 by $\lambda_{\bar{U}}$ with $\bar{U}$ being the mean depth-averaged current below the wave trough for each profile. A comparison of λ_m and $\lambda_{\bar{U}}$ provides the simplest assessment of the importance of vorticity in the flow field.

The influence of vorticity is greatest for the profiles presented when the current is weakest and strongest, corresponding to figures 3 and 7. In both of these figures the velocity profiles for the finite-amplitude irrotational wavetrain with constant current $\bar{U}$ are shown by dot-dash lines and it is clear that the vorticity distribution is an important property for both wavelength and velocity predictions. The vorticity distribution for the mean flows in figures 3 and 7 is globally influential and not confined to narrow shear layers. In figure 3, $U(z)$ does not contain any regions of strong vorticity and $U(z)$ appears to change smoothly over the whole range; however, $U(z)$ cannot be well modelled by a uniform current nor by one with uniform vorticity. For the profile in figure 7 there is a strong shear layer near to the bed but a reasonable approximation to the other points can be obtained using a least-squares straight-line fit to the data. This straight-line fit corresponds to a current with a uniform vorticity distribution and the wavelength for this constant vorticity profile predicted by the numerical model is 1.850 m, which is seen from table 2 to be a reasonable estimate of the wavelength, and the same is true of the corresponding velocity predictions.

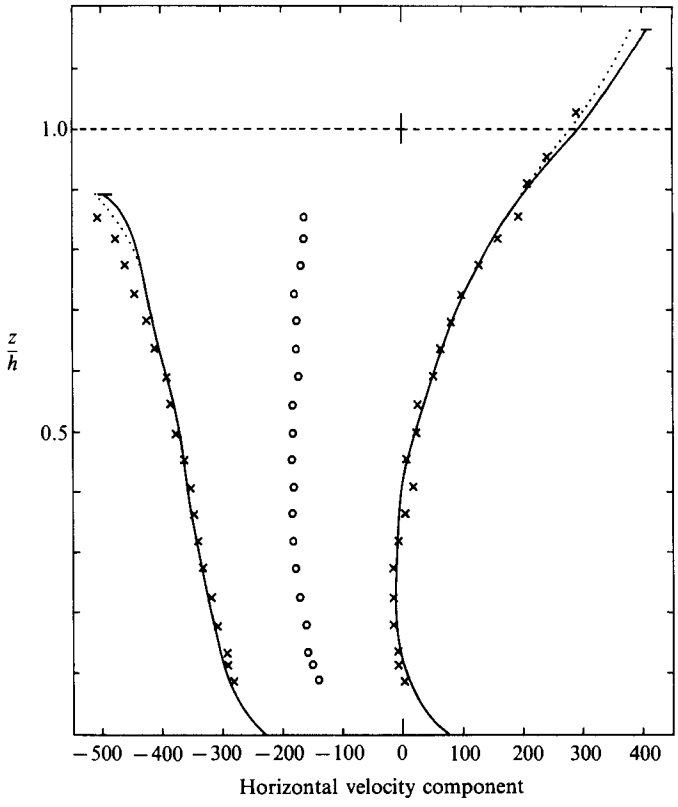

FIGURE 6. As for figure 3, with $\bar{U} = -166.53$ mm/s.

For figures 4–6 the irrotational theory provides a reasonable approximation to both wavelength and velocity profiles. They do not provide agreement to the same degree of accuracy as the numerical model but are surprisingly good. In these cases the velocity profiles are well described by irrotational approximations except near the bed where there are pronounced shear layers. However, the dominant feature is that the currents are globally irrotational and hence the applicability of the irrotational model. An examination of a region containing a strong shear layer, such as the range $-1.0 < z/h < -0.8$ in figure 5, confirms that the local variations in velocity cannot be predicted accurately using the irrotational theory.

The importance of the global distribution of vorticity has been demonstrated above. However, the numerical model contains a dependence not just upon the vorticity distribution but also upon the way the vorticity changes via higher-order wave contributions. The quantity λ_{p_1} which appears in table 2 is the wavelength prediction using the first-order vorticity distribution as described by (4.12). If λ_{p_1} is regarded as the first-order approximation, then λ_p as presented here is the next-order approximation and essentially provides a fine-tuning mechanism. Both λ_p and λ_{p_1} will usually give good estimates for the wavelengths; the prediction λ_p is usually slightly better than λ_{p_1} and this is most noticeable for the strongest current. The velocity predictions for the present profiles corresponding to λ_{p_1} are almost always very close to those corresponding to the full numerical model and λ_p; the exceptions usually occur near to the free surface and these are shown in the figures by dotted lines. However, the constraint is more difficult to implement with the first-order

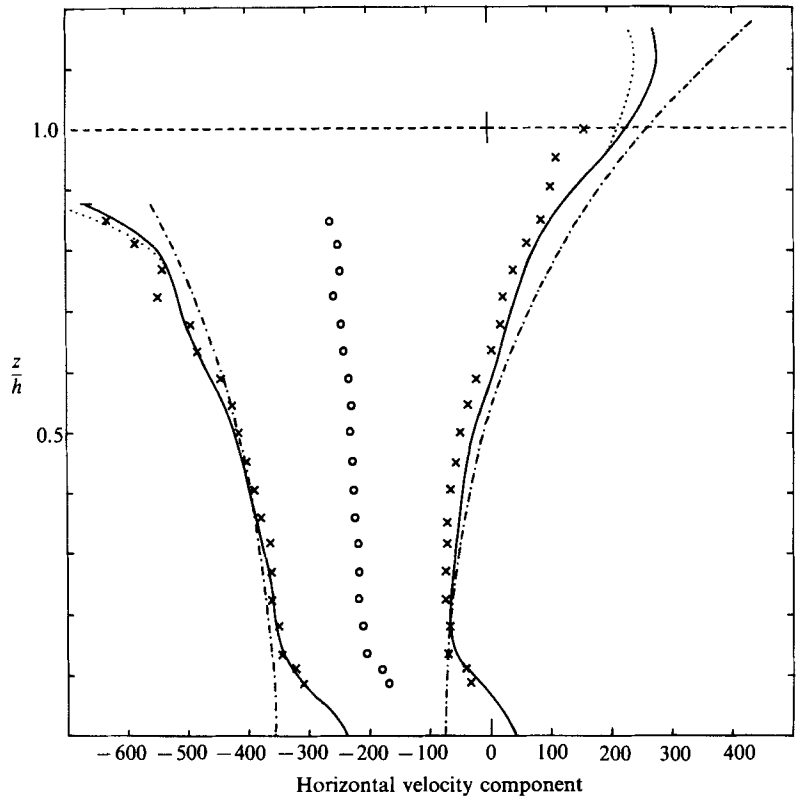

FIGURE 7. As for figure 3, with $\bar{U} = -218.09$ mm/s.

vorticity approximation and for the profiles studied the mean constraint error was up to four times that of the full numerical model, with the maximum individual error always occurring close to the free surface.

These experimental results confirm the validity of the present model and demonstrate the importance of the global vorticity distribution.

9. Slowly varying properties of the flow

The experimental results described in the previous section can also be used to investigate the slowly varying properties of the flow in a similar manner to that described by Thomas (1981) for linear wave–current interactions.

The waves in the experiments were all generated on still water of depth 0.55 m at the same fixed frequency using the same paddle displacement. In the absence of pump-generated currents the velocity profiles of figure 3 would be reproduced in each case. When a current is present each of the interactions illustrated in figures 4–7 is justifiably regarded as being locally constant. The sequence of interactions is viewed as a set of windows on a continually changing process in which the current becomes increasingly adverse owing to upwelling from below in the slowly varying sense, i.e. changes in the current occur over a scale of many wavelengths. For the experimental facility the current generating mechanism causes changes in the current to occur over lengthscales of the order of one wavelength and strictly speaking the slowly varying theory is not valid. However, with this difficulty acknowledged and in the absence

of a more suitable theory, good agreement was shown to exist by Thomas (1981) between predictions using the Whitham (1974) theory and experimental results for interactions between linear waves and essentially irrotational currents.

For linear waves on a current with uniform vorticity, defined by $U(z) = U_s + \Omega z$, the conservation relations that govern the amplitude and wavelength variations are

$$\left.\begin{aligned} (\omega - kU_s)^2 &= [gk - \Omega(\omega - kU_s)] \tanh kh, \\ \frac{E}{\omega - k\bar{U}} c_g &= \text{constant}, \end{aligned}\right\} \tag{9.1}$$

where E is the mean energy density of the waves, c_g is the group velocity and $\bar{U}$ is the depth-averaged current, i.e. $\bar{U} = U_s - \frac{1}{2}\Omega h$. The first relation in (9.1) is the local dispersion relation and the second is often referred to as the conservation of wave action. If $\Omega = 0$ then the flow is irrotational with $E = \frac{1}{2}\rho g a^2$ and the simplified form of (9.1) is due to Longuet-Higgins & Stewart (1961) for deep water and more generally to Bretherton & Garrett (1968). When $\Omega \neq 0$, E is a complicated function of the wave and current parameters and the appropriate expression was derived by Jonsson, Brink-Kjaer & Thomas (1978). There is at present no analogue of (9.1) for a general rotational current. A nonlinear form of (9.1) exists only for a current with zero vorticity.

The experimental results of figures 4–6 have been shown to be reasonably well predicted for both wavelength and velocity profiles by assuming the current profile to be irrotational, though the predictions are not as accurate as those of the full numerical model. For figures 3 and 7 the vorticity distribution is globally important and the irrotational approximation does not work very well. This suggests that a nonlinear analogue of (9.1) may describe some of the amplitude and wavelength variations quite well, but that others will probably not be so well represented.

Following Crapper (1979) the average Lagrangian L for a nonlinear wavetrain and mean flow U is written, with density ρ omitted, as

$$L = (\gamma - \tfrac{1}{2}U^2)\, h - \tfrac{1}{2}gh^2 + L_w, \tag{9.2}$$

where γ is the Bernoulli constant and L_w is due to the waves alone. The slight difference between (9.2) and the form given by Crapper is due to a difference in the choice of the position of the coordinate origin; the form (9.2) is appropriate for water of mean depth h when the bottom is horizontal.

If theory consistent with the Stokes fifth-order theory is to be used, then L_w must be determined correct to $O(a^6)$. The derivation of L_w correct to $O(a^4)$ has been given by Whitham (1974, p. 555). Using a similar derivation but extended to higher order gives

$$L_w = -\tfrac{1}{4}ga^2\{1 + \tfrac{1}{2}(ak)^2 c_1(kh) + \tfrac{1}{3}(ak)^4 c_2(kh)\} + \frac{a^2(\omega - kU)^2}{4k \tanh kh} + O(ak)^8, \tag{9.3}$$

where the coefficients $c_1(kh)$ and $c_2(kh)$ are the same as those given by Skjelbreia & Hendrickson (1960), i.e.

$$c_1(kh) = (9T^4 - 10T^2 + 9)/8T^4,$$

$$c_2(kh) = (3840 - 4096S^2 + 2592S^4 - 1008S^6 - 5944S^8 - 1830S^{10} + 147S^{12})/512T^{10}(5 + T^2),$$

where $T = \tanh kh$ and $S^2 = 1 - T^2$.

The modulations in the wavelength and wave amplitude are governed by the equations

$$\frac{\partial L}{\partial a} = 0, \quad \frac{\partial L}{\partial k} = 0 \tag{9.4}$$

and it is clear from (9.2) that only L_w will contribute to these. The first of these gives

$$(\omega - kU)^2 = gk \tanh kh[1 + (ak)^2 c_1(kh) + (ak)^4 c_2(kh)] \tag{9.5}$$

which is the local dispersion relation as well as a global conservation relation.

The second relation in (9.4) is the conservation of wave action equation, which is written most simply as

$$\frac{a^2}{k}[F_1(kh, U) + (ak)^2 F_2(kh, U) + (ak)^4 F_3(kh, U)] = \text{constant}, \tag{9.6}$$

where

$$F_1(kh) = \tfrac{1}{2} + \frac{kh}{\sinh 2kh} + \frac{kU}{(gk \tanh kh)^{\frac{1}{2}}},$$

$$F_2(kh) = c_1\left\{1 + \frac{kh}{\sinh 2kh} + \frac{kU}{2(gk \tanh kh)^{\frac{1}{2}}}\right\} + \frac{k}{4}\frac{\partial c_1}{\partial k},$$

$$F_3(kh) = c_2\left\{\frac{7}{6} + \frac{kh}{\sinh 2kh} + \frac{kU}{2(gk \tanh kh)^{\frac{1}{2}}}\right\} + \frac{k}{6}\frac{\partial c_2}{\partial k} - \frac{kUc_1^2}{8(gk \tanh kh)^{\frac{1}{2}}}.$$

Note that $F_1(kh)$ is the group velocity to local phase speed ratio for linear waves. If a reference position is described by a, h, k and U having the values a_0, h_0, k_0 and U_0 respectively, then (9.6) can be written as

$$\left(\frac{a}{a_0}\right)^2 = \frac{k}{k_0}\left\{\frac{F_1(k_0 h_0, U_0) + (a_0 k_0)^2 F_2(k_0 h_0, U_0) + (a_0 k_0)^4 F_3(k_0 h_0, U_0)}{F_1(kh, U) + (ak)^2 F_2(kh, U) + (ak)^4 F_3(kh, U)}\right\}. \tag{9.7}$$

The two relations (9.5) and (9.7) are coupled but are sufficient to describe the amplitude and wavelength variations. Suppose for fixed frequency ω that a suitable reference set a_0, h_0, U_0 is known and that the data set $\{(h_i, U_i), i = 1, \ldots, N\}$ is given. The first step is to determine k_0 using (9.5). For each pair of values of (h_i, U_i), the value of a/a_0 and k/k_0 is then determined simultaneously from (9.5) and (9.7).

The reference data point is chosen to correspond to the profile in figure 5 with $\bar{U} = -118.01$ mm/s; the data from table 2 gives $a_0 = 69.94$ mm and $\lambda_0 = \lambda_{\bar{U}} = 2.090$ m. The predicted value of the wavelength rather than the measured value must be used because the dispersion relation (9.5) must be satisfied. All of the required data for the measured values of a/a_0 and $\lambda/\lambda_0\,(= k_0/k)$ are available from table 2 and the predicted values are obtained using (9.5) and (9.7). The results are displayed graphically in figure 8 and tabulated in table 3.

Comparison of the measured and predicted wave amplitude and wavelength variations in figure 8 and table 3 shows surprisingly good agreement between the two sets of data. It had been previously anticipated that the data from figures 4–6 might fit the irrotational theory reasonably well and for this reason the reference point was chosen to correspond to figure 5. However, the data points corresponding to figures 3 and 7, for which the vorticity has been established as an important factor in the local wave–current interactions, appear in figure 8 as part of a general pattern rather than taking isolated values. The general pattern established by the experimental

Figure	$\bar{U}$ (mm/s)	Measured a/a_0	Predicted a/a_0	Measured λ/λ_0	Predicted λ/λ_0
3	14.44	0.922	0.886	1.094	1.112
4	−85.69	0.985	0.969	1.018	1.027
5	−118.01	1.000	1.000	0.997	1.000
6	−166.53	1.035	1.048	0.961	0.958
7	−218.09	1.083	1.105	0.877	0.916

TABLE 3. The measured and predicted values of the non-dimensional wave amplitude and wavelength. The experimental data are taken from table 2 and the predicted values derived using equations (9.5) and (9.7). In the notation of table 2, a_0 and λ_0 correspond the values of a and $\lambda_{\bar{U}}$ when $\bar{U} = -118.01$ mm/s

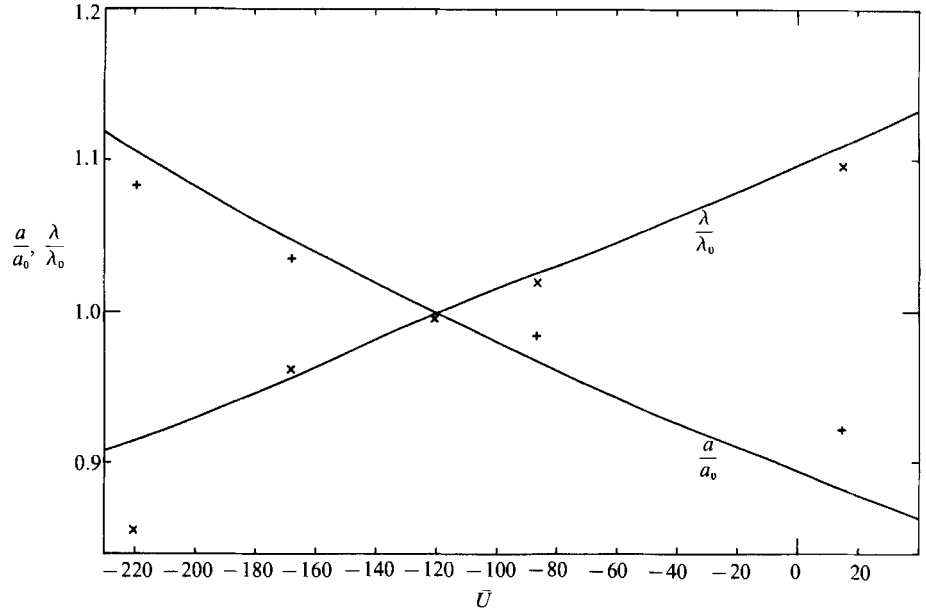

FIGURE 8. The predicted and experimentally obtained values of the non-dimensional wave amplitude a/a_0 and wavelength λ/λ_0 plotted against the depth-averaged mean current $\bar{U}$ (measured in mm/s). The data are given in table 3: ——, theoretical curves; ×, experimentally measured wavelengths; +, experimentally measured wave amplitudes.

data is reasonably close to the predicted curves, though the relative position of theoretical and experimental values must depend upon the reference point chosen.

It cannot be deduced that the irrotational theory will provide a similar degree of accuracy for wave amplitude and wavelength variations when the current profiles possess a greater distribution of vorticity. The discrepancy between the experimental values and theoretical curves in figure 8 may well be due in part to neglect of vorticity, in addition to other likely contributory factors such as beach and current reflections and experimental measurement errors. It has previously been mentioned that the slowly varying theory is not strictly valid as the experimental facility forces the current to change over a distance of the order of a wavelength and it is readily acknowledged that this and the preceding factors will play possibly important roles but which are difficult to quantify. Consideration of all these various mechanisms

strengthens the initial impression that the agreement in figure 8 is surprisingly good, even though the linear result (9.1) hints at the central role played by the mean current $\bar{U}$.

10. Conclusions

Good agreement has been shown to exist between the predictions of a numerical model and experimentally measured values of the wavelength and velocity profiles associated with a finite-amplitude wavetrain interacting with a steady current containing an arbitrary distribution of vorticity.

The experimental results obtained, together with existing finite-amplitude theories, demonstrate the importance of the global vorticity distribution in the wave–current interaction. If the current profile is essentially irrotational with vorticity restricted to thin layers, then the irrotational theory will provide a reasonable approximation for both wavelengths and velocities except in the vicinity of the shear layer. For flows with a global distribution of vorticity, the vorticity will have an important influence on the wavelength and velocities. In such cases the irrotational theories can only be used if the vorticity distribution is approximately constant as this corresponds to an irrotational wave field. When the vorticity is globally important and not uniformly distributed the full numerical method should be used although some approximation can be made for vorticity distributions which do not contain regions of rapid change.

A slowly varying approach for finite-amplitude waves on constant currents was employed in conjunction with the experimental results. Moderate agreement was obtained between theory and experiment, with the maximum discrepancy occurring for those currents with influential global vorticity distributions. The agreement was encouraging and confirms the importance of the depth-averaged mean flow in determining the amplitude and wavelength modulations. In addition to the presence of vorticity in the current distributions, a second difficulty was associated with the implementation of the slowly varying theory. The theory assumes that any changes in the wave and current properties occur over a scale of several wavelengths. In this application changes in the current occurred over a lengthscale of approximately one wavelength and thus the slowly varying theory is not strictly valid. Given the twin difficulties of vorticity and regime validity the theory provided surprisingly good estimates for the amplitude and wavelength variations.

The experimental results described in this paper were obtained when the author was a member of the School of Mathematics, University of Bristol, using facilities made available in the Hydraulics Laboratory of the Department of Civil Engineering. To the Department of Civil Engineering for providing facilities, and the SERC for providing financial support, the author wishes to express his gratitude.

Appendix A. The equation for $\psi_n(z)$

In a frame of reference moving with the wave, the condition that the vorticity is constant along a streamline gives $(u-c)\Omega_x + w\Omega_z = 0$. With the stream function $\psi(x,z)$ defined by (2.3) and ψ related to Ω by the Poisson equation (2.4), the condition becomes

$$\psi_x(\nabla^2\psi)_x = \psi_z(\nabla^2\psi)_x. \tag{A 1}$$

For $-h \leqslant z \leqslant z_t$ a solution is sought of the form given by (3.14):

$$\psi(x,z) = c(z+h) - \int_{-h}^{z} U(z)\,\mathrm{d}z + \sum_{n=1}^{\infty} \psi_n(z)\cos nkx. \tag{A 2}$$

Although this form is only assumed to exist for the range given, the usual practice in linear and near-linear wave theories is to assume that this is valid up to the position of the mean value of the free surface.

Substitution from (A 2) into (A 1) and matching harmonic components gives

$$2(U-c)\,nk\left[\psi_n'' - \left\{\frac{U''}{U-c} + (nk)^2\right\}\psi_n\right] = \sum_{m=1}^{\infty} (D_{m+n,\,m} - D_{m,\,m+n}) + \sum_{m=1}^{n+1} D_{m,\,n-m}, \quad n = 1,2,\ldots,$$

where $D_{m,q} = mk\{\psi_q[\psi_m'' - (mk)^2\psi_m] - \psi_m[\psi_q'' - (qk)^2\psi_q]\}$ and a prime denotes differentiation with respect to z.

A more convenient form of this system of equations is

$$\psi_n'' - \left\{\frac{U''}{U-c} + (nk)^2\right\}\psi_n = g_n(z), \quad n = 1,2,\ldots, \tag{A 3}$$

where $$g_n(z) = \frac{1}{2nk(U-c)}\left\{\sum_{m=n+1}^{\infty} D_{m,\,m-n} + \sum_{m=1}^{\infty} (D_{m+n,\,m} - D_{m,\,m+n})\right\}.$$

This is equation (4.4).

Appendix B

The equation (A 3) cannot be solved exactly using analytical techniques. Fortunately in the present application only the form of the functions $g_n(z)$ is of interest and so solution of the system of equations is not necessary.

Suppose that ϵ is some small parameter for the flow, such as the wave slope. In keeping with existing theories for weakly nonlinear waves, an expansion for $\psi_n(z)$ is sought of the form

$$\psi_n(z) = \epsilon^n[\psi_{n0}(z) + \epsilon\psi_{n1}(z) + \epsilon^2\psi_{n2}(z) + \ldots], \quad n = 1,2,\ldots. \tag{B 1}$$

Thus each $\psi_n(z)$ is of $O(\epsilon^n)$, but each $\psi_{nj}(z)$ is of $O(1)$ $(j = 0,1,2,\ldots)$. Each of the functions $g_n(z)$ must be expanded similarly,

$$g_n(z) = \epsilon^n[g_{n0}(z) + \epsilon g_{n1}(z) + \epsilon^2 g_{n2}(z) + \ldots], \quad n = 1,2,\ldots. \tag{B 2}$$

Substitution from (B 1) and (B 2) into (A 3) and equating equal powers of ϵ gives

$$\psi_{nj}'' - \left\{\frac{U''}{U-c} + (nk)^2\right\}\psi_{nj} = g_{nj} \tag{B 3}$$

as the system of equations to determine $\psi_{nj}(n = 1,2,\ldots, j = 0,1,2,\ldots)$. The appropriate method of solution for such a system, with regard to the structure of g_{nj}, is to first determine $\psi_{n0}(n = 1,2,\ldots)$, then $\psi_{n1}(n = 1,2,\ldots)$ and so on.

The form of each function $g_{nj}(z)$ can be determined from (A 3) with the expansions

(B 1) and (B 2) inserted. If the functions ψ_{nj} are determined in the order prescribed above then the g_{nj} are composed of previously determined functions.

Solutions are sought which are correct to third order and so have an error of $O(\epsilon^4)$. This necessitates determination of the functions g_{nj} for which $n+j \leqslant 3$. These are straightforward to obtain but the algebra is tedious. In their simplest forms, the six relevant functions are given by

$$\left.\begin{aligned} g_{10} &= g_{11} = 0, \quad g_{20} = -\frac{\psi_{10}}{4(U-c)}[\ ]', \\ g_{12} &= \frac{1}{2(U-c)}\{-\psi_{20}\psi_{10}[\ ]' + 2g_{20}\psi'_{10} + \psi_{10}g'_{20}\}, \\ g_{21} &= -\frac{1}{2(U-c)}\psi_{10}\psi_{11}[\ ]', \\ g_{30} &= \frac{1}{2(U-c)}\{-\psi_{20}\psi_{10}[\ ]' + \tfrac{1}{3}[2g_{20}\psi'_{10} - \psi_{10}g'_{20}]\}, \end{aligned}\right\} \tag{B 4}$$

where $[\ ] = U''/(U-c)$.

Simplification is possible for the function $g_2(z) = \epsilon^2 g_{20} + \epsilon^3 g_{21} + \ldots$ to the degree of accuracy employed. As $\psi_1(z) = \epsilon\psi_{10} + \epsilon^2\psi_{11} + \ldots$ and $\psi_1^2 = \epsilon^2[\psi_{10}^2 + 2\epsilon\psi_{10}\psi_{11} + \ldots]$, it is clearly seen using (B 4) that

$$g_2(z) = -\frac{\psi_1^2}{4(U-c)}\left[\frac{U''}{U-c}\right]' + O(\epsilon^4). \tag{B 5}$$

Appendix C. The series $G(x_0, z_0)$

In §4 the series $G(x, z)$ is defined to be

$$G(x, z) = \sum_{n=1}^{\infty} g_n(z)\cos nkx. \tag{C 1}$$

For a given value of $z = z_0$, x_0 is the value of x at which

$$\sum_{n=1}^{\infty} \psi_n(z_0)\cos nkx_0 = 0. \tag{C 2}$$

As $\psi_n(-h) = 0$ for all n, it can be assumed that $z_0 > -h$. With $\psi_n(z_0)$ given by (B 1), it is relatively easy to show that the solution x_0 of (C 2) satisfies

$$\cos kx_0 = O(\epsilon), \quad \cos 2kx_0 = -1 + O(\epsilon^2), \quad \cos 3kx_0 = O(\epsilon).$$

Substitution for $g_n(x)$ from (B 2) and (B 4) yields

$$\begin{aligned} G(x_0, z_0) &= -\epsilon^2[g_{20} + \epsilon g_{21}] + O(\epsilon^4) \\ &= -g_2(z_0) + O(\epsilon^4). \end{aligned}$$

But $g_2(z)$ is given by (B 5) and hence

$$G(x_0, z_0) = \frac{\psi_1^2(z)}{4(U-c)}\left[\frac{U''}{U-c}\right]' + O(\epsilon^4), \tag{C 2}$$

which is the result used in (4.7).

Appendix D. The series $G(\pi/k, z_t)$

This series appears in (4.9) and is simply $-g_1(z_t)+g_2(z_t)-g_3(z_t)+\ldots$. With the expansion given in (B 2) all of the necessary terms are listed in (B 4). Making use of the form for $g_2(z)$ given in (B 5), the series is

$$G\left(\frac{\pi}{k}, z_t\right) = -\frac{\psi_1^2}{4(U-c)}\left[\frac{U''}{U-c}\right]' - \epsilon^3[g_{12}(z)+g_{30}(z_t)]+O(\epsilon^4) \quad \text{at} \quad z=z_t. \tag{D 1}$$

In the expressions for g_{12} and g_{30} the functions $\epsilon\psi_{10}$ and $\epsilon^2\psi_{20}$ can be replaced by ψ_1 and ψ_2 respectively without any loss in accuracy of (D 1). An alternative and expanded form of (D 1) is

$$G\left(\frac{\pi}{k}, z_t\right) = -\frac{1}{4(U-c)}(\psi_1^2-4\psi_1\psi_2)[\,]' + \frac{\psi_1^2}{6(U-c)}\left\{\frac{\psi_1'}{(U-c)}[\,]' - \frac{\psi_1}{2}\left(\frac{[\,]}{U-c}\right)'\right\}$$
$$+O(\epsilon^4) \quad \text{on} \quad z=z_t. \tag{D 2}$$

The boundary condition to be applied on $z=z_t$ is given by (3.13),

$$\psi_1-\psi_2 = \alpha h + cz_t + O(\epsilon^3).$$

Unfortunately this cannot be combined with (D 2) to give an expression in which ψ_1 and ψ_2 do not appear and which is correct to third order.

However, if an order of magnitude is sacrificed then the substitution $\psi_1 = \alpha h + cz_t$ will give

$$G\left(\frac{\pi}{k}, z_t\right) = -\frac{(\alpha h+cz_t)^2}{4(U-c)}\left[\frac{U''}{U-c}\right]' + O(\epsilon^3)$$

and this is the expression which appears in (4.10).

REFERENCES

BENJAMIN, T. B. 1962 The solitary wave on a stream with an arbitrary distribution of vorticity. *J. Fluid Mech.* **12**, 97–116.

BRETHERTON, F. P. & GARRETT, C. J. R. 1968 Wavetrains in inhomogeneous moving media. *Proc. R. Soc. Lond.* A **302**, 529–554.

BREVIK, I. 1980 Flume experiment on waves and currents, II, Smooth bed. *Coastal Engng* **4**, 89–110.

BREVIK, I. & AAS, B. 1980 Flume experiment on waves and currents, I, Rippled bed. *Coastal Engng* **3**, 149–177.

CRAPPER, G. D. 1979 Energy and momentum integrals for progressive capillary–gravity waves. *J. Fluid Mech.* **94**, 13–24.

DALRYMPLE, R. A. 1973 Water wave models and wave forces with shear currents. *Coastal and Ocean Engng Lab., Univ. of Florida, Tech. Rep.* 20.

DALRYMPLE, R. A. 1974 A finite amplitude wave on a linear shear current. *J. Geophys. Res.* **79**, 4498–4504.

DALRYMPLE, R. A. 1977 A numerical model for periodic finite amplitude waves on a rotational fluid. *J. Comput. Phys.* **24**, 29–42.

DUBREIL-JACOTIN, M. L. 1934 Sur la determination regoureuse des ondes permanentes periodiques d'amplitude finie. *J. Math.* **13**, 217–291.

FENTON, J. D. 1985 A fifth order Stokes theory for steady waves. *J. Waterway, Port, Coastal and Ocean Eng. Div. ASCE* **111**, 216–234.

GREIG, D. M. 1980 *Optimisation.* Longman.

HANSEN, J. B. & SVENDSEN, I. A. 1974 Laboratory generation of waves of constant form. *Proc. 14th Coastal Engng Conf.*, pp. 321–339. ASCE.

JONSSON, I. G., BRINK-KJAER, O. & THOMAS, G. P. 1978 Wave action and set-down for waves on a shear current. *J. Fluid Mech.* **87**, 401–416.

KEMP, P. H. & SIMONS, R. R. 1982 The interaction between waves and a turbulent current: waves propagating with the current. *J. Fluid Mech.* **116**, 227–250.

KEMP, P. H. & SIMONS, R. R. 1983 The interaction of waves and a turbulent current: waves propagating against the current. *J. Fluid Mech.* **130**, 73–89.

LONGUET-HIGGINS, M. S. & STEWART, R. W. 1961 Changes in amplitude of short gravity waves on steady non-uniform currents. *J. Fluid Mech.* **10**, 529–549.

PEREGRINE, D. H. 1976 Interaction of water waves and currents. *Adv. Appl. Mech.* **16**, 9–117.

PEREGRINE, D. H. & JONSSON, I. G. 1983 Interaction of waves and currents. *Rep.* MR 83-6. CERC.

ROACHE, P. J. 1982 *Computational Fluid Dynamics.* Albuquerque: Hermosa.

SIMMEN, J. A. & SAFFMAN, P. G. 1985 Steady deep-water waves on a linear shear current. *Stud. Appl. Maths* **73**, 35–57.

SKJELBREIA, L. & HENDRICKSON, J. 1960 Fifth order gravity wave-theory. *Proc. 7th Coastal Engng Conf.*, pp. 321–339. ASCE.

TELES DA SILVA, A. F. & PEREGRINE, D. H. 1988 Steep, steady surface waves on water of finite depth with constant vorticity. *J. Fluid Mech.* **195**, 281–302.

THOMAS, G. P. 1981 Wave–current interactions: an experimental and numerical study. Part 1. Linear waves. *J. Fluid Mech.* **110**, 457–474.

WHITHAM, G. B. 1974 *Linear and Nonlinear Waves.* Wiley-Interscience.